Toward an Understanding of Vertical Momentum Transports in Cloud-System-Resolving Model Simulations of Multiscale Tropical Convection

TIFFANY A. SHAW

Department of Earth and Environmental Sciences, and Department of Applied Physics and Applied Mathematics, Columbia University, New York, New York

TODD P. LANE

School of Earth Sciences, and ARC Centre of Excellence for Climate System Science, The University of Melbourne, Parkville, Victoria, Australia

(Manuscript received 22 February 2013, in final form 17 April 2013)

ABSTRACT

This study examines the characteristics of convective momentum transport (CMT) and gravity wave momentum transport (GWMT) in two-dimensional cloud-system-resolving model simulations, including the relationships between the two transports. A linear group velocity criterion is shown to objectively separate CMT and GWMT. The GWMT contribution is mostly consistent with upward-propagating gravity waves and is present in the troposphere and the stratosphere. The CMT contribution forms a large part of the residual (nonupward-propagating contribution) and dominates the fluxes in the troposphere. Additional analysis of the vertical sensible heat flux supports the physical interpretation of the two contributions, further isolating the effects of unstable convection from vertically propagating gravity waves.

The role of transient and nonconservative (friction and diabatic heating) processes in generating momentum flux and their dependence on changes in convective organization was assessed using a pseudomomentum budget analysis. Nonconservative effects were found to dominate the transports; the GWMT contribution involved a diabatic source region in the troposphere and a dissipative sink region in the stratosphere. The CMT contribution was consistent with transport between the boundary layer and free troposphere via tilted convection. Transient buoyancy–vorticity correlations highlighted wave sources in the region of convective outflow and the boundary layer. These sources were akin to the previously described ''mechanical oscillator'' mechanism. Fluxes associated with this upper-level source were most sensitive to convective organization, highlighting the mechanism by which changes in organization are communicated to GWMT. The results elucidate important interactions between CMT and GWMT, adding further weight to suggestions that the two transports should be linked in parameterizations.

1. Introduction

The vertical flux of horizontal momentum on mesoscales in the atmosphere is associated with two important processes: 1) convective momentum transport (CMT), which is the transport associated convective updrafts, convective downdrafts, and coherent tilted structures associated with mesoscale organization (Moncrieff 1992), and 2) gravity wave momentum transport (GWMT), which is the transport associated with vertically propagating gravity waves (Fritts and Alexander 2003). CMT occurs primarily in the troposphere, and it has been shown to be significant both in field campaigns (LeMone 1983; LeMone et al. 1984) and as a residual term in the tropical momentum budget in reanalysis data (Carr and Bretherton 2001; Lin et al. 2005). Several recent studies have shown that including parameterized CMT in a general circulation model improves the modeled Hadley circulation and the intraseasonal and interannual variability in the tropical troposphere (Zhang and McFarlane 1995; Wu et al. 2003, 2007; Richter and Rasch 2008). GWMT occurs between wave generation regions in the troposphere and wave dissipation regions in the troposphere, stratosphere, and mesosphere. The main sources are from orography, convection, fronts, and jets. Parameterized

Corresponding author address: Dr. Tiffany A. Shaw, Department of Earth and Environmental Sciences and Department of Applied Physics and Applied Mathematics, Columbia University, P.O. Box 1000, 61 Route 9W, Palisades, NY 10964.
E-mail: tas2163@columbia.edu

DOI: 10.1175/JAS-D-13-068.1

GWMT is required to properly simulate the general circulation of the middle atmosphere (Fritts and Alexander 2003). Although both CMT and GWMT are recognized as important processes, they are typically treated independently in models even though convection is known to simultaneously transport momentum within the troposphere and generate gravity waves that transport momentum aloft. In particular, CMT and GWMT are currently parameterized independently in climate models.

Understanding the connection between CMT from GWMT is challenging on many levels. Both processes are associated with convection and depend on the mode of convective organization. In addition, both processes occur in the troposphere and may interact and are therefore difficult to separate. Most studies of the vertical momentum transport by convection typically focus on either CMT or GWMT. For example, studies of GWMT have focused on the generation of vertically propagating gravity waves by time-varying convection through the so-called diabatic heat source, mechanical oscillator, or topographic mechanisms [for a review, see Fritts and Alexander (2003)]. The generated gravity waves propagate upward into the middle atmosphere; however, downward propagation from elevated sources is also possible. In contrast, studies of CMT have focused on how it influences the surrounding environment through tilted convective structures (Moncrieff 1992) and meridional circulations. Recently, Lane and Moncrieff (2010, hereafter LM10) analyzed the connection between GWMT and CMT in two-dimensional cloud-system-resolving model simulations. They focused primarily on two vertical levels: one in the lower troposphere (2.5 km) and one in the upper stratosphere (20 km). These levels essentially isolated CMT and GWMT, and showed that the two processes display a consistent sign of the momentum transports. The consistency in sign was linked to the preferential generation of gravity waves whose phase lines contained the same tilt as the organized convective structures.

LM10 has shed light on the interaction between CMT and GWMT; however, many questions remain. Outstanding questions include: can CMT and GWMT be objectively separated? What are the primary sources of the two contributions (e.g., transient growth or decay of wave amplitude or diabatic heat source effects)? What is the process through which changes in CMT translate to changes in GWMT? The main purpose of this paper is to better understand the connection between CMT and GWMT by answering these questions, which are addressed using two-dimensional cloud-system-resolving model simulations of multiscale tropical convection. In particular, we seek to objectively separate the two contributions via a linear group velocity criterion with additional insight from analysis of sensible heat transports. To understand the role of transient changes and diabatic effects in the generation of GWMT and CMT we appeal to the wave-activity conservation law for disturbances to a vertically varying shear-stratified flow. Such conservation laws relate the momentum flux divergence to nonconservative processes such as diabatic heating, friction or transient growth, or decay of wave activity density, which is proportional to wave amplitude. The budget is used to study momentum transports by convection and gravity waves simultaneously, which helps elucidate their connections.

The remainder of the paper is organized as follows: Section 2 discusses the two-dimensional cloud-system-resolving model simulations and wave-activity diagnostics. The separation of the momentum fluxes into upward-propagating gravity wave and nonupward-propagating contributions is also discussed. Section 3 discusses the vertical pseudomomentum transfers in the absence of background wind. In section 4 the transfers in the presence of low-level eastward wind shear, which acts to organize the convection, are discussed. The results are summarized and discussed in section 5.

2. Cloud-system-resolving model simulations and diagnostics

a. Model description

The cloud-system-resolving model used in this study is the anelastic model of Clark et al. (1996). The domain is two-dimensional, 2000 km wide and 40 km deep with horizontal grid spacing $\Delta x = 1$ km and vertical grid spacing that varies from $\Delta z = 50$ m near the surface to 200 m aloft. The uppermost 10 km of the model domain includes a Rayleigh drag sponge layer and the lateral boundaries are periodic. The imposed thermodynamic sounding was observed over the Tiwi Islands, Australia (see Fig. 1, left), and is the same as that used in LM10. The x direction is aligned in the east–west direction and rotation is neglected. The imposed zonal wind is either zero, for example, $U(z) = 0$ labeled UNS (U-no shear), or is negative below 3.5 km, labeled USH (U-shear, see Fig. 1, right). The USH wind profile is given by the following analytical expression:

$$U(z) = \begin{cases} -a\left\{\cos\left[\dfrac{\pi(z+2.5)}{1.2H}\right] - \cos\left[\dfrac{2\pi(z+2.5)}{1.2H}\right]\right\} - 2a, & z \le 3.5\ \text{km} \\ 0, & z > 3.5\ \text{km}, \end{cases} \tag{1}$$

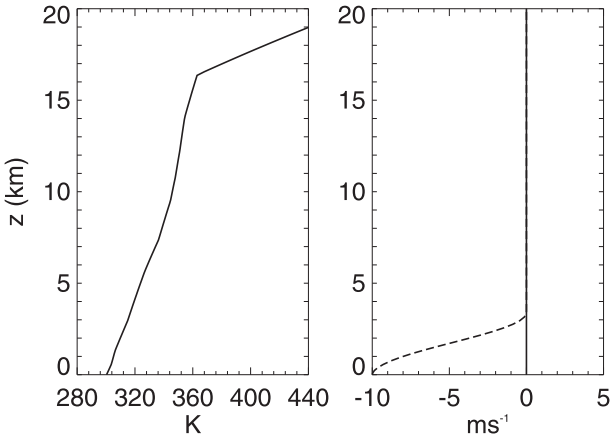

FIG. 1. (left) Background potential temperature profile and (right) horizontal wind. The horizontal wind was prescribed as either zero (UNS, solid) or with an eastward wind shear below 3.5 km (USH, dashed).

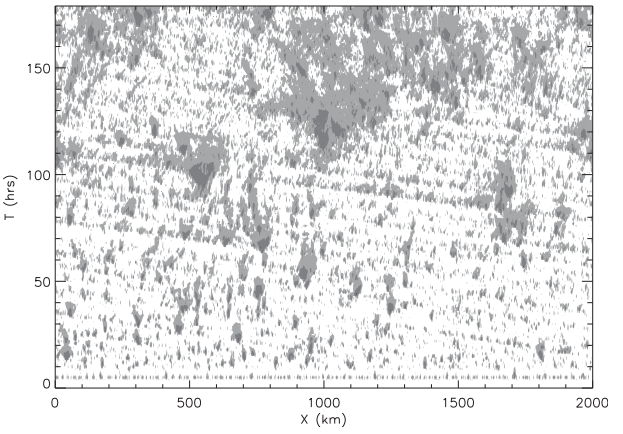

FIG. 2. Total-column cloud (shaded) from the cloud-system-resolving model simulations for USH.

where $a = 3.2$ and $H = 5$ km. The shear profile is similar to the U10 profile used by LM10 but is smoother and the vertical shear is continuous. Each simulation is run for 180 h with a 5-s time step. The data is recorded every 2 min along with the data at the subsequent time step so that the time derivative terms could be accurately calculated. Convection is maintained by constant surface fluxes of latent ($100\,\mathrm{W\,m^{-2}}$) and sensible ($10\,\mathrm{W\,m^{-2}}$) heat and an imposed cooling of $2\,\mathrm{K\,day^{-1}}$ below 9.5 km that decreases linearly in magnitude to $0\,\mathrm{K\,day^{-1}}$ at 15.5 km. These surface fluxes and internal cooling help to sustain convection, which approaches a near-equilibrium state; nonetheless, the flow never achieves a true steady state (even in the mean), allowing analysis of transient processes. Lane and Moncrieff (2008), LM10, and Lane and Zhang (2011) analyzed multiscale convection and gravity waves in UNS. Figure 1 in LM10 shows the evolution of the vertically integrated cloud water in UNS as a function of time. Figure 2 shows the evolution of the integrated cloud water as a function of time for the USH simulation.

b. Upward- versus nonupward-propagating waves

As discussed previously, the vertical flux of horizontal momentum includes contributions from both CMT and GWMT. An important distinction between the two transports is that GWMT is typically associated with upward-propagating gravity waves. Here we will use a criterion based on linear wave theory to separate spectral components that are consistent with upward wave (energy) propagation from those that are not. Spectral components are determined by applying a Fourier transform to the horizontal space and time coordinates at every vertical level. The criterion for upward propagation is based on the so-called first Eliassen–Palm (EP) theorem (Eliassen and Palm 1961; Lindzen 1990), that is,

$$c_p\rho_0\Theta\overline{\pi' w'} = -\rho_0(U-c)\overline{u'w'} = \rho_0 c_{gz}\langle E\rangle, \qquad (2)$$

for anelastic dynamics, where c_p is the specific heat at constant pressure; $\rho_0(z)$ and $\Theta(z)$ are the background density and potential temperature, respectively; c is the phase speed in the x direction; π', w', and u' are the disturbance Exner function, horizontal, and vertical wind, respectively; c_{gz} is the vertical group velocity; and $E = \rho_0|\mathbf{v}'|^2/2 + \rho_0 g\theta'^2/2\theta_0\Theta_z$ is the wave energy with $|\mathbf{v}'|$ the disturbance wave velocity, which is averaged over phase indicated by the angle brackets. According to linear theory, spectral elements that have a positive pressure flux have a positive vertical group velocity (because ρ_0 and E are positive definite) and therefore represent upward-propagating waves. The remaining spectral components represent the nonupward-propagating contribution. Note that the nonupward-propagating contribution may include momentum transport by convection and downward-propagating gravity waves. The decomposition is consistent with LM10, who separated CMT and GWMT using the relationship between the sign of the momentum flux and phase speed, which is equivalent to (2) for $U = 0$.

The decomposition into upward- and nonupward-propagating contributions is applied using the cospectrum of the pressure and vertical velocity perturbations, which determines the pressure flux for each spectral component. The sign of these pressure fluxes are used as a filter in spectral space that isolates the upward and nonupward contributions, which is applied to other

spectra throughout this study such as the momentum transport and the pseudomomentum density. A key question is whether the decomposition into upward and nonupward contributions using a criterion from linear wave theory is sufficient to separate CMT from GWMT in nonlinear simulations.

c. Wave-activity diagnostics

To address questions regarding the role of transient and diabatic effects in generating convective momentum transport and gravity wave momentum transport and how changes in CMT affect GWMT, we need a framework that explains how the vertical flux of horizontal momentum is changing in time and space. A framework for understanding the evolution of momentum transports by disturbances to some background flow defined by a time, space, or ensemble average is a wave-activity conservation law. The conservation law states that the wave-activity density A is conserved in the absence of nonconservative processes; for example,

$$\frac{\partial A}{\partial t} + \nabla \cdot \mathbf{F} = 0, \tag{3}$$

where $\mathbf{F}$ is the wave-activity flux. The flux term includes the vertical flux of horizontal momentum, that is, CMT and GWMT. In the presence of nonconservative processes, such as diabatic heating and friction, a source/sink term S can be added to the rhs of (3) (Haynes 1988).

Here we are interested in characterizing how the momentum flux associated with two-dimensional disturbances to a vertically dependent shear-stratified background flow evolves. The background flow relevant for the cloud-system-resolving model simulations consists of the background wind $U(z)$, vorticity $\Omega(z)$, and potential temperature $\Theta(z)$. Scinocca and Shepherd (1992, hereafter SS92) derived the pseudomomentum wave-activity conservation laws for two-dimensional anelastic (and Boussinesq) disturbances to a shear-stratified flow. Their formulation was based on the anelastic model of Lipps and Hemler (1982) [see (3.1)–(3.3) in SS92] and considered dry, conservative dynamics. Note that the Lipps and Hemler formulation is the basis of the Clark et al. (1996) model. According to SS92, the wave-activity density and flux for two-dimensional anelastic disturbances are

$$A = \Gamma(\Theta)\theta'\omega' + (\Omega - \omega')\int_0^{\theta'} [\Gamma(\Theta + \eta) - \Gamma(\Theta)]\, d\eta - \rho_0 \int_0^{\theta'} [\Pi(\Theta + \eta) - \Pi(\Theta)]\, d\eta, \tag{4a}$$

$$F_{(x)} = \frac{\rho_0}{2}[(u')^2 - (w')^2] + (U + u')A + \frac{g}{\theta_0}\int_0^{\theta'}\left[\int_{\Theta}^{\Theta+\eta} \Gamma(\xi)d\xi\right] d\eta, \tag{4b}$$

$$F_{(z)} = \rho_0 u'w' + w'A, \tag{4c}$$

$$S = S^{\theta}\{\Gamma(\Theta)\omega' + (\Omega - \omega')[\Gamma(\Theta + \theta') - \Gamma(\Theta)] - \rho_0[\Pi(\Theta + \theta') - \Pi(\Theta)]\} \tag{4d}$$

$$+ S^{\omega}\left[\int_0^{\theta'} \Gamma(\Theta + \eta)\, d\eta\right], \tag{4e}$$

where ω', θ' are the disturbance vorticity and potential temperature, respectively; $\Gamma(\Theta) = \rho_0 dz/d\Theta$ and $\Pi(\Theta) = \Omega dz/d\Theta$ [see (6.10) and (6.21) of SS92], where $\rho_0(z)$ is the background density with $\Theta = p_0/R\rho_0\pi_0$ and $c_p\Theta d\pi_0/dz = -g$ (see SS92 section 3). Finally, $D\theta/Dt = S^{\theta}$ and $D\omega/Dt + g\partial\theta/\partial x/\theta_0 = S^{\omega}$, with D/Dt representing a Lagrangian (or total) derivative; S^{θ} and S^{ω} are the nonconservative terms in the potential temperature and vorticity equations, respectively.

The first term in the pseudomomentum density A in (4a) involves the product of the disturbance buoyancy and vorticity, which is known to be important for wave generation by penetrative convection (Lane 2008). The second term also involves the product of the buoyancy and vorticity but includes an integral measuring the degree to which the flow has been driven away from the background state. The third term in the pseudomomentum density depends directly on the background vorticity through Π and in the small-amplitude limit is proportional to the squared potential temperature disturbance $-\Gamma^2 d(\Omega/\rho_0)/dz(\theta')^2/2$ [see (6.15) in SS92]. The horizontal component of the pseudomomentum flux $F_{(x)}$ in (4b) involves the horizontal flux of horizontal momentum, vertical flux of vertical momentum, and terms associated with the advection of the pseudomomentum density by the background and disturbance horizontal wind. The vertical component of the pseudomomentum flux $F_{(z)}$ in (4c) involves the familiar vertical flux of horizontal momentum and a term associated with the advection of the pseudomomentum density by the disturbance vertical wind. We will refer to the first term in the vertical flux in (4c), equal to the vertical flux of horizontal momentum, as the linear vertical pseudomomentum flux following Scinocca and Peltier (1994) because it is the flux determined from a solution of the linearized equations [see (5.23) of SS92]. Note that the familiar Eliassen–Palm flux is related to the vertical flux of horizontal pseudomomentum. The remaining term in the vertical pseudomomentum

flux, equal to the advection of the pseudomomentum density by the disturbance wind, is associated with nonlinearities; that is, it is cubic. The source/sink term in (4e) can be derived following section 2 of appendix C in SS92.

The term of interest in the pseudomomentum wave-activity conservation law is the linear vertical pseudomomentum flux, which includes both CMT and GWMT. We are particularly interested in the x-averaged vertical divergence since that is what needs to be parameterized in climate models. The x-averaged vertical divergence of the linear vertical pseudomomentum flux can be isolated in the wave-activity conservation law so as to understand the cause of the flux divergence:

$$\frac{\partial}{\partial z}(\rho_0\overline{u'w'}) = \overline{S} - \frac{\partial}{\partial z}(\overline{w'A}) - \frac{\partial \overline{A}}{\partial t} \tag{5a}$$

$$= \tilde{\overline{S}} - \frac{\partial \overline{A}}{\partial t}, \tag{5b}$$

where the overbar represent an x average and $\tilde{S}$ is the effective source/sink term. The terms on the rhs of (5a) are associated with (in order) nonconservative effects, nonlinearity due to the advection of the pseudomomentum density by the disturbance vertical wind, and transience of the pseudomomentum density. The nonlinear flux terms are combined with the source/sink term to create an effective source/sink term. This is consistent with previous studies that have shown that both diabatic effects and transient nonlinear terms act to generate gravity waves and, thus, a vertical flux of horizontal momentum (Song et al. 2003). In the analysis that follows we will use (5b) to understand the cause of the vertical divergence of horizontal momentum.

It is important to note that, although the model simulation approaches a mean state near equilibrium, it never achieves a steady state because of the ongoing transient convection. The mean of the transient term in (5b) exposes this nonsteady mean state. More importantly, however, the spectral analysis of the transient term (presented later) identifies the transient signals that combine (and mostly cancel) to form the mean state. Where the spectral components of the transient term are large identifies those altitudes dominated by transient wave generation and dissipation.

When interpreting the cause of the vertical divergence of horizontal momentum we can also draw analogies to the application of wave-activity conservation laws to a transient baroclinic life cycle. The life cycle involves a source region near the surface and a sink region in the upper troposphere where the waves are dissipated. A full description can be found in Held and Hoskins (1985) and Edmon et al. (1980). During the baroclinic life cycle the wave amplitude grows via instability and waves propagate vertically away from the surface. The propagation away from the surface leads to a decay of wave amplitude in that region and thus a flux divergence; for example, $\mathbf{\nabla} \cdot \mathbf{F} \approx -\partial A/\partial t > 0$. In the midtroposphere the waves propagate vertically conserving wave-activity and there is zero flux divergence; for example, $\mathbf{\nabla} \cdot \mathbf{F} \approx 0$. Once the waves reach the tropopause they propagate meridionally, producing another region of divergence. The waves are dissipated through irreversible wave breaking that produces a flux convergence on poleward and equatorward sides of the divergence region in the upper troposphere, which is balanced by a sink term such as diffusion; for example, $\mathbf{\nabla} \cdot \mathbf{F} \approx S < 0$. The baroclinic life cycle clearly shows that transience can induce momentum flux divergence if wave activity is growing or decaying in time, for example, when waves are being generated by a transient source, if waves are dissipated by some transient wave breaking process, or if wave packets are propagating through a region of space. Here we apply the wave-activity conservation law to assess the role of transience versus diabatic and friction terms in generating the linear vertical pseudomomentum flux in the cloud-resolving model experiments. This approach helps to isolate wave generation via the ''mechanical oscillator'' (transient penetrating convective updraft) and ''diabatic heat source'' (quasi-stationary thermal forcing) effects.

3. Momentum transfers in the absence of background wind shear

As a starting point for understanding the relationship between CMT and GWMT, we consider the transport in the absence of background wind shear. In the simulation with no background wind shear (UNS), shallow convection develops initially and eventually self-organizes into clusters, which propagate without a preferred direction (see Fig. 1 in LM10). Further details on the convective evolution can be found in Lane and Moncrieff (2008), LM10, and Lane and Zhang (2011). We consider the evolution during two 50-h periods: 20–70 and 120–170 h, which effectively separates the organized and disorganized stages of the system evolution.

a. Decomposition into upward- and nonupward-propagating signals

Figure 3 (top) shows the vertical flux of horizontal momentum divided by density $u'w'$ as a function of phase speed c and height for the two 50-h periods (left and right, respectively). To create this, the vertical flux of horizontal momentum is determined using the cospectrum of the disturbance horizontal and vertical

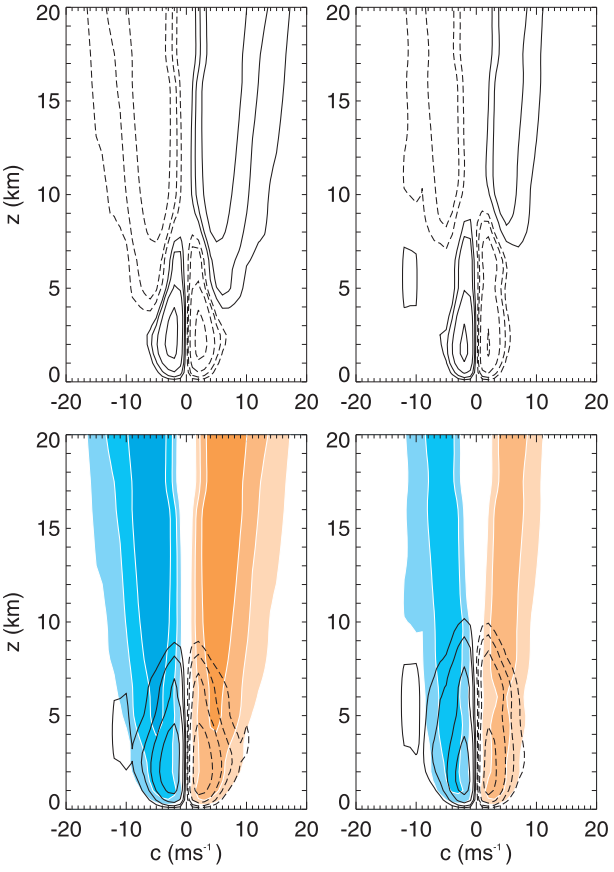

FIG. 3. Phase speed spectrum vs height during (left) 20–70 and (right) 120–170 h for (top) the vertical flux of horizontal momentum divided by density and (bottom) the spectrum separated into upward (color)- and nonupward (black)-propagating contributions for UNS. Contour values are $\pm 10 \times (4, 8, 16, 32, 64, \text{etc.})$ $\text{m}^2\,\text{s}^{-1}\,\text{day}^{-1}$ $(\text{m}\,\text{s}^{-1})^{-1}$; negative contours are dashed or blue.

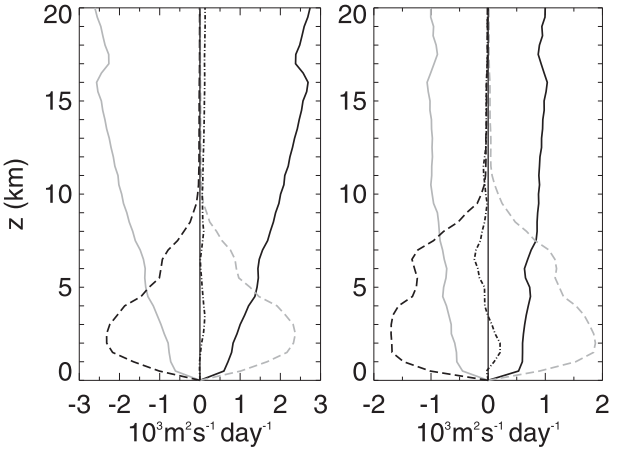

FIG. 4. Evolution during (left) 20–70 and (right) 120–170 h of the UNS vertical flux of horizontal momentum divided by density, shown in Fig. 3, integrated over $c > U$ (black) and $c < U$ (gray) phase speed for upward (solid) and nonupward (dashed) contributions. The domain average flux is dashed–dotted.

wind, and each spectral element is sorted into $1\,\text{m}\,\text{s}^{-1}$ wide phase speed bins. The spectra were calculated at 0.5-km vertical intervals, which extends beyond the LM10 analysis. During the two time periods, the spectra are nearly antisymmetric about zero phase speed at all vertical levels. The net vertical flux of horizontal momentum changes sign with height and there are opposite signed extrema at 2 km for $|c| = 2\,\text{m}\,\text{s}^{-1}$ and 15.5 km for $|c| = 5\,\text{m}\,\text{s}^{-1}$ as noted by LM10 (see their Fig. 5). For $c > U = 0$ ($c < U = 0$) phase speeds, the net flux is negative (positive) in the lower troposphere and is positive (negative) aloft. Note that in the absence of background wind a spectral element that contains phase speed and vertical flux of horizontal momentum of the same sign is consistent with upward gravity wave propagation [see (2)].

Next we consider the separation of the vertical flux of horizontal momentum using the upward-wave-propagation criteria from linear theory. Figure 3 (bottom) shows the separation of the vertical flux of horizontal momentum into upward (color)- and nonupward (black)-propagating contributions using the pressure flux method discussed in section 2b. The upward-propagation filter suggests that the momentum transport signals associated with positive pressure flux occurs from the surface to the upper stratosphere, consistent with what we expect for upward-propagating gravity waves. The spectra for the upward contribution is nearly antisymmetric about zero but with phase speeds ranging from $|c| = 4$ to $6\,\text{m}\,\text{s}^{-1}$. The nonupward contribution is confined to the troposphere, consistent with what we expect of CMT and convective structures. The spectra for the nonupward contribution is nearly antisymmetric about zero with peak phase speeds of $|c| = 3\,\text{m}\,\text{s}^{-1}$. The differences in the upward and nonupward spectra are consistent with LM10, who based their decomposition on the relationship between the sign of the momentum flux and phase speed instead of calculating the pressure flux directly.

Figure 4 shows the integral of the vertical flux of horizontal momentum in Fig. 3 over $c > U = 0$ (black) and $c < U = 0$ (gray) phase speeds, including their upward (solid) and nonupward (dashed) contributions during the two 50-h periods. The domain-averaged flux is small and reflects small breaks in the antisymmetry of the spectrum that occur as the cloud field periodically becomes dominated by long-lived propagating disturbances. The upward flux weakens at upper levels as the simulation progresses. This is consistent with weaker vertical wind within the convection at later times (Lane and Moncrieff 2008). Note that the upward and nonupward contributions overlap below 10 km, with the nonupward contribution dominating below 7 km. This transition region between 7 and 10 km is where wave

generation by overshooting convection might be expected to dominate.

The upward-propagation criterion from linear theory appears to successfully separate transport between the stratosphere and troposphere from that confined to the troposphere. Previous work (e.g., LM10) has shown that the momentum transports within organized convective systems are often (but not always) of opposite sign to the system propagation velocity. This property underlies the assumption that CMT makes the dominant contribution to the nonupward signals in the troposphere; however, downward-propagating gravity waves may also be important. A clearer understanding of the dominance of convection in the nonupward contribution can be achieved by considering the cospectrum of the vertical sensible heat flux, for example, the cospectrum of the potential temperature θ' and the vertical wind w'. Recall that the vertical sensible heat flux for a gravity wave in the absence of nonconservative processes, such as diabatic heating, radiation, and friction, is exactly zero. However, in the presence of nonconservative processes the vertical sensible heat flux is expected to be negative (downgradient). In contrast, the vertical sensible heat flux for unstable moist convection is expected to be positive (upgradient). Figure 5 (top) shows the vertical sensible flux as a function of phase speed and height for the two 50-h periods (left and right, respectively) for UNS. The net vertical sensible heat flux is positive below 10 km, consistent with convective transport, and negative above 10 km, consistent with downgradient mixing. The spectrum is nearly symmetric about zero phase speed. Figure 5 (bottom) shows the decomposition of the sensible heat flux spectra into upward (color) and nonupward (black) contributions using the pressure-flux-based filter. The nonupward contribution is mostly positive, consistent with convective transport, and dominates below 12 km. In contrast, the upward contribution is mostly negative from the surface up to 20 km, consistent with downgradient transport. Overall, the decomposition suggests that the upward-propagating contribution is associated with downgradient sensible heat transport, which is due to resolved and numerical diffusion that damps vertically propagating gravity waves. The nonupward contribution is primarily associated with convection that transports heat upgradient.

While the net nonupward contribution to the sensible heat transport is positive and suggestive of convective transport, it does not rule out the possibility of negative sensible heat transport that would be consistent with downward-propagating waves. To quantify the role of downward-propagating waves we separate the nonupward vertical sensible heat flux into negative (color) and positive (black) contributions (Fig. 6, top). The

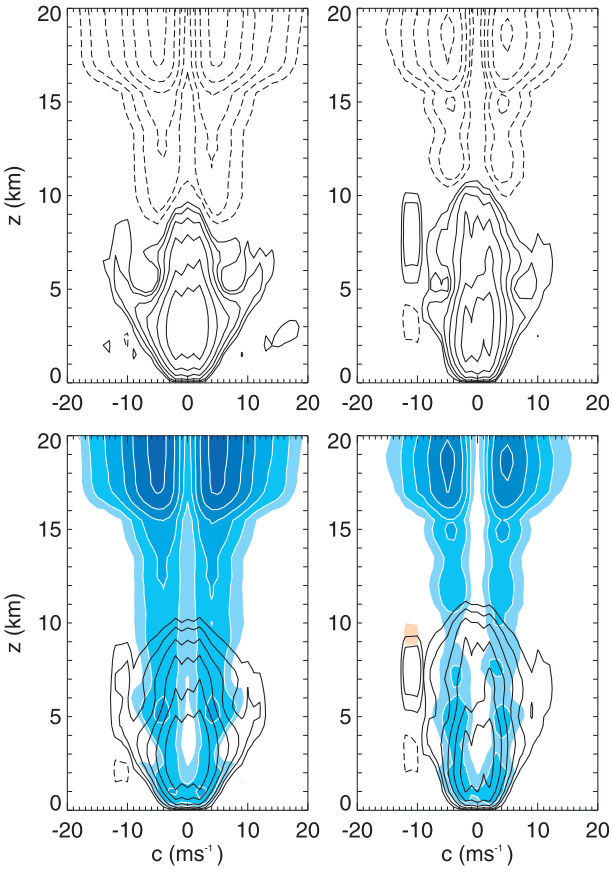

FIG. 5. Phase speed spectrum vs height during (left) 20–70 and (right) 120–170 h for (top) the vertical sensible heat flux and (bottom) the spectrum separated into upward (color)- and nonupward (black)-propagating contributions for UNS. Contour values increase/decrease in powers of 2; for example, $\pm$(4, 8, 16, 32, 64, etc.) K m day^{-1} (m s^{-1})$^{-1}$; negative contours are dashed or blue.

negative flux is clearly nonzero and suggests that the net nonupward sensible heat transport does include downward-propagating gravity waves. The contribution of downward-propagating waves to the vertical flux of horizontal momentum can be assessed by separating the nonupward momentum flux (Fig. 3, bottom, black) into contributions associated with positive and negative vertical sensible heat flux. Figure 6 (bottom) shows the decomposition of the nonupward vertical flux of horizontal momentum into spectral elements with negative (color) and positive (black) sensible heat flux contributions. The positive heat flux contribution to the nonupward vertical flux of horizontal momentum clearly dominates. Thus, the nonupward momentum flux is largely due to convection or some kind of convectively coupled gravity waves with $\theta' w' > 0$. The remaining contribution from downward-propagating gravity waves with $\theta' w' < 0$ is small.

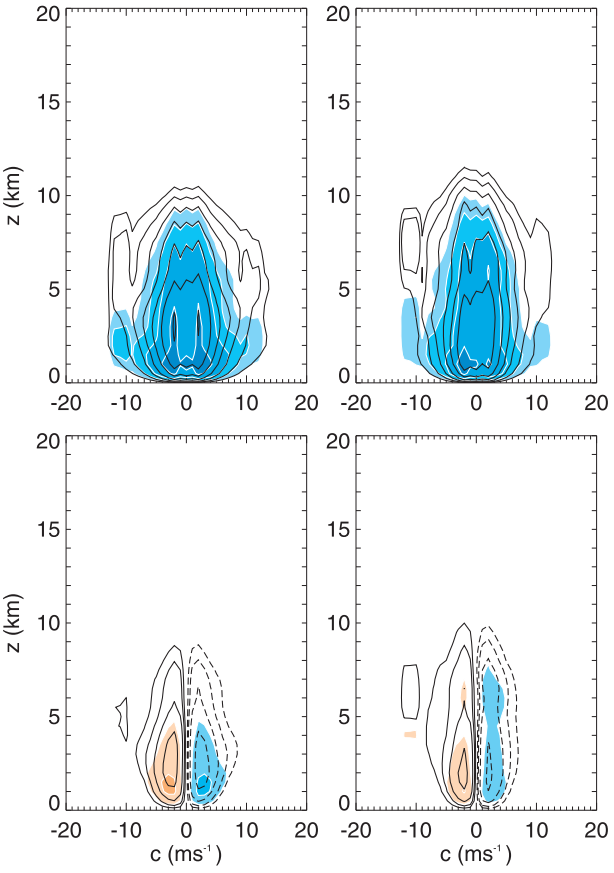

FIG. 6. Phase speed spectrum vs height during (left) 20–70 and (right) 120–170 h of (top) the nonupward vertical sensible heat flux separated into negative (color) and positive (black) contributions for UNS. Contouring as in Fig. 5. (bottom) The nonupward vertical flux of horizontal momentum divided by density (see black contours in Fig. 3) separated into negative (color) and positive (black) sensible heat flux contributions for UNS. Contouring as in Fig. 3.

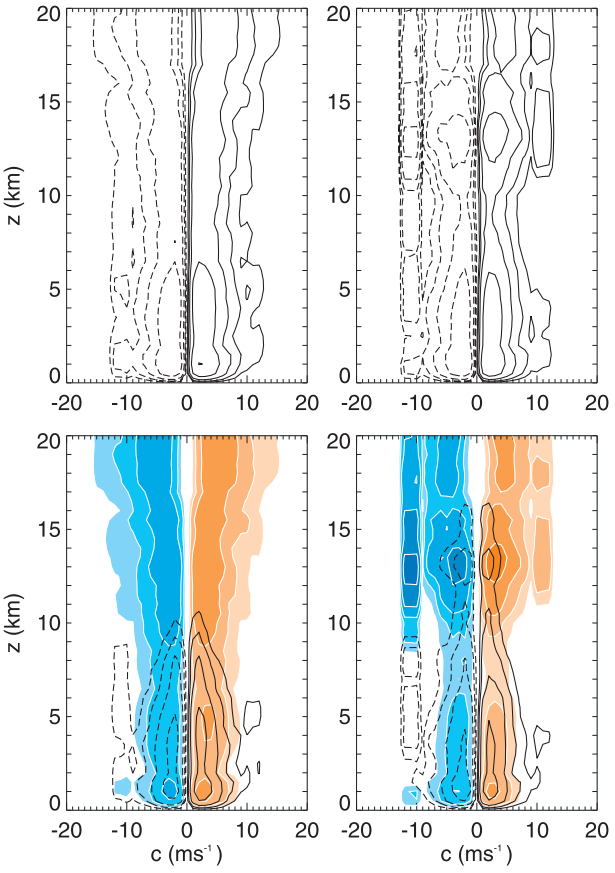

FIG. 7. As in Fig. 3, but for the pseudomomentum density divided by density A/ρ_0 for UNS. Contour values are $\pm 10^{-4} \times (1, 2, 4, 8, 16, 32, 64, \text{etc.})$ m^2 s^{-1} (m s^{-1})$^{-1}$; negative contours are dashed or blue.

Thus, using a spectral filter based on the first EP theorem derived from linear theory, the aforementioned spectral analysis has successfully separated the momentum fluxes associated with upward- and downward-propagating waves from those momentum flux signals derived from convective motions. The analysis suggests that the answer to the question posed in the introduction "Can CMT and GWMT be objectively separated?" is "yes" in the absence of background shear. The application of the upward-propagating wave filter helps disentangle the vertical structure of the momentum transport and its evolution. Of course, the processes within the convection are inherently nonlinear and the possibility of nonlinear wave–wave interactions also exists. Yet, the separations are sufficiently clear, which suggests that the filter derived from linear theory is adequate for the purposes herein.

b. *Pseudomomentum budget analysis of UNS*

To understand the evolution and source of momentum transport in the troposphere and stratosphere, we appeal to the pseudomomentum wave-activity conservation law outlined in section 2c. In all of the simulations presented here the horizontal pseudomomentum flux in (4b) was found to be very weak compared to the other terms in (5a) and, therefore, it is not shown. We begin with the pseudomomentum wave-activity density because the pseudomomentum flux has no meaning in the absence of the density. Note that in the absence of background wind shear (e.g., $\Omega = 0$), the pseudomomentum density A only involves the first two terms in (4a) and the first term is found to dominate. Figure 7 (top) shows the pseudomomentum density divided by density, that is, $A \approx \Gamma(\Theta)\theta' w'$, as a function of phase speed and height for the two 50-h periods (left and right, respectively). Regions with large pseudomomentum density indicate where buoyancy and vorticity are correlated. Note that both convection and gravity waves can induce buoyancy–vorticity correlations. The pseudomomentum

density is large from the surface to the upper stratosphere and is nearly symmetric about zero phase speed. An important point to note is that the pseudomomentum density is single signed at all vertical levels for a given phase speed. During the first 50-h extrema exist at 3 km, similar to the vertical flux of horizontal momentum, which is likely related to the main convective region of storms. In the last 50-h period during the time of deepest convection in the simulation a second extremum appears between 10 and 15 km. These vertical locations coincide with the region of convective outflow. The upward- and nonupward-propagation decomposition of the pseudomomentum density is shown in Fig. 7 (bottom). The decomposition is consistent with that for the vertical flux of horizontal momentum; namely, the nonupward contribution dominates in the troposphere and the upward contribution dominates aloft.

The wave-activity conservation law states that changes in the vertical flux of horizontal momentum result from either transience of the pseudomomentum density (transient changes in wave amplitude) or source/sink terms (diabatic and frictional effects) [see (5b)]. Figure 8 (top) shows the negative time tendency of the pseudomomentum divided by density, for example, $-\partial A/\partial t/\rho_0$ [second term on the rhs of (5b)], as a function of phase speed and height for the two 50-h periods (left and right, respectively). Overall, the transience term is small but does exhibit extrema below 5 km and between 10 and 15 km in the vicinity of convective outflow, with the latter developing in the last 50-h period. The sign of the transience term is consistent with a local divergence associated with transient decay of pseudomomentum density (or wave amplitude). The physical interpretation is that transient processes are generating waves at the altitudes highlighted by the extrema. The low altitudes ($z < 5$ km) are likely associated with shallow convection, and the higher altitudes ($10 < z < 15$ km) correspond to regions of overshooting convection. Many previous studies (e.g., Fovell et al. 1992; Lane et al. 2001) have shown that overshooting convection generates gravity waves via a transient process commonly referred to as the mechanical oscillator effect. The waves generated in this region propagate away, producing a flux divergence, similar to the divergence by Rossby waves in the extratropical upper troposphere (see Held and Hoskins 1985, Figs. 3 and 6). Figure 8 (bottom) shows the decomposition of the transience term into upward- and nonupward-propagating contributions. Overall, the upward contribution dominates, suggesting transience is a source of upward-propagating waves at all vertical levels. As the simulation evolves, the upward contribution increases between 10 and 15 km, suggesting enhanced wave generation. This increase between 10 and 15 km occurs in the region of convective outflow, where buoyancy–vorticity correlations are large and episodic (see Fig. 7, bottom), and appears to isolate the region of wave generation by penetrative convection.

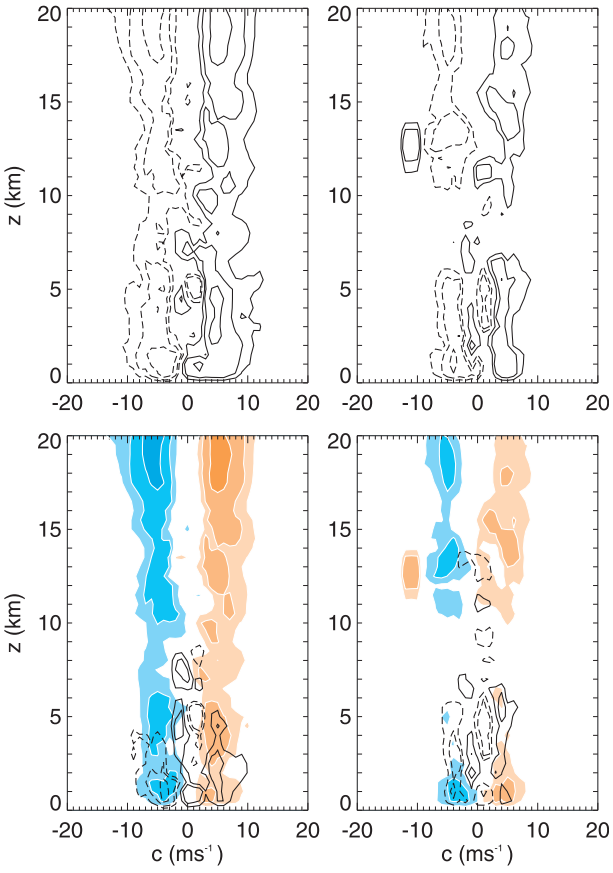

FIG. 8. As in Fig. 3, but for the transience of the pseudomomentum density divided by density $-\partial A/\partial t/\rho_0$ for UNS. Contour values are $\pm 10^{-4} \times (4, 8, 16, 32, 64, \text{etc.})$ m s^{-1} day^{-1} (m s^{-1})$^{-1}$; negative contours are dashed or blue.

The remaining contribution to the vertical divergence of the vertical flux of horizontal momentum is the effective source/sink term $\tilde{S}$ [see the first term on the rhs of (5b)]. As discussed previously, the effective source/sink term includes both nonconservative (diabatic heating and friction) and nonlinear terms. Here the nonconservative contribution is found to dominate over the nonlinear contribution (not shown). Figure 9 (top) shows the effective source/sink term divided by density $\tilde{S}/\rho_0$ as a function of phase speed and height for the two 50-h periods (left and right, respectively). The vertical structure of the source/sink term has many qualitative similarities with the vertical flux of horizontal momentum. The physical interpretation of its vertical structure becomes clearer after the upward and nonupward contributions are separated (Fig. 9, bottom). The upward-propagating contribution involves a dipole structure from

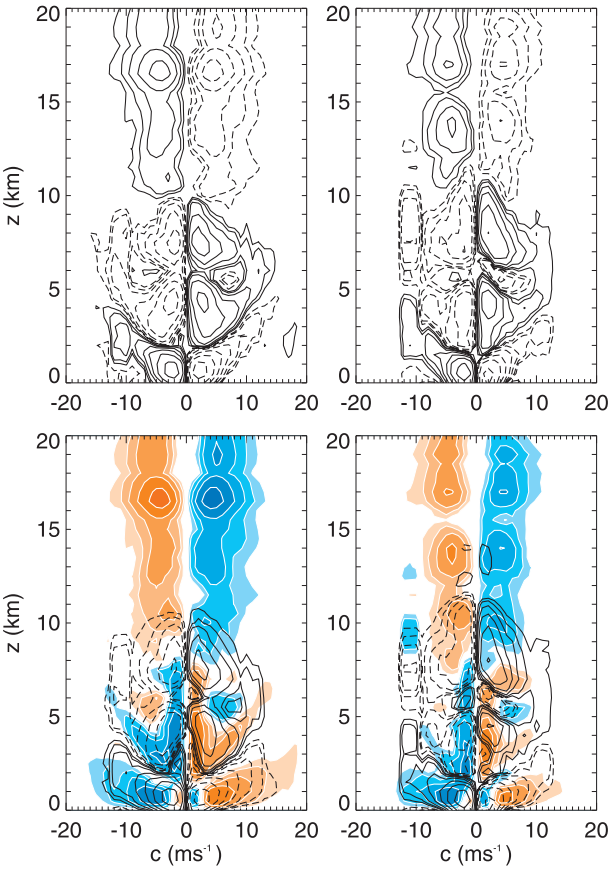

FIG. 9. As in Fig. 3, but for the pseudomomentum effective source/sink term divided by density $\tilde{S}/\rho_0$ for UNS. Contouring as in Fig. 8.

the surface up to 20 km. For $c > U$ ($c < U$) there is a region of divergence (convergence) below a region of convergence (divergence). In the generation region ($z < 10$ km) the diabatic heating dominates the nonconservative term (i.e., S^{θ}), whereas in the dissipation region ($z > 10$ km) the friction dominates the nonconservative term (e.g., S^{ω}) (not shown). Thus, the pattern diagnosed from the (quasi steady) source/sink term is suggestive of the generation of upward-propagating waves by the diabatic heating in the lower to midtroposphere, which leads to vertical wave propagation and dissipation in the upper troposphere and lower stratosphere.[1] In contrast, the nonupward contribution has an opposite signed dipole with height. Its vertical structure is suggestive of vertical transport of horizontal momentum between the boundary layer and the lower to midtroposphere. The notion of vertical propagation between regions of generation and dissipation is not appropriate in this case as tilted convection can induce such vertical transport.

Overall, the application of the upward-propagation filter and wave-activity conservation law diagnostic to the UNS simulation has provided insight into CMT and GWMT in the absence of background wind shear. The wave-activity conservation law analysis reveals that the upward-propagating contribution to the vertical flux of horizontal momentum is largely consistent with gravity wave dynamics and its parameterization (Lindzen 1990; Fritts and Alexander 2003). For a given phase speed spectral element there is a generation region (below approximately 10 km in this case) that generates upward-propagating gravity waves that are subsequently dissipated aloft (above approximately 10 km). The generation by diabatic forcing dominates and results primarily from the correlation of the vorticity and the diabatic heating [e.g., (4e)]. This diabatic source can be explained by the "diabatic heat source" effect (Alexander et al. 1995). A separate source region is identified by the transience of the pseudomomentum associated with convective overshoot at the level of storm outflow. This transient source can be explained by the "mechanical oscillator" effect Fovell et al. (1992), which has been shown to be related to nonlinear body forces (e.g., Lane et al. 2001). On the other hand, the nonupward contribution to the vertical flux of horizontal momentum suggests that the nonupward transport can also be considered wavelike and is consistent with propagating convective systems with circulations that are tilted. For example, a positively tilted convective complex produces a positive flux of horizontal momentum that transfers momentum from the boundary layer into the free troposphere. A negatively tilted convective complex produces a negative flux of horizontal momentum that transfers momentum from the free troposphere into the boundary layer. Once again, the vertical flux of horizontal momentum is dominated by the correlation of the diabatic heating and the vorticity (the transience term is very weak). The pseudomomentum budget reveals that there is significant overlap between the upward and nonupward momentum transport contributions, suggesting that they are not separable in terms of their regions of influence. These ideas are extended to simulations with low-level wind shear in the next section.

4. Momentum transfers in the presence of low-level wind shear

When a background low-level negative wind shear is applied to the two-dimensional cloud-system-resolving model simulations (USH), the convection becomes

[1] The region of wave dissipation at 17 km is related to numerical resolution. When the vertical resolution was increased the amount of dissipation decreased, suggesting that a very high vertical resolution is required to resolve the change in vertical wavelength across the tropopause.

more organized (see Fig. 2); it transitions from upshear propagating (downshear tilt) to quasi stationary (upright tilt) and finally to cloud clusters (upshear tilt) (see also Fig. 11 in LM10). The evolution of the convection is consistent with the development of mesoscale convective systems that are known to occur in the presence of low-level wind shear (e.g., Houze 2004). LM10 noted changes in both CMT and GWMT in the presence of low-level wind shear, including enhanced westward GWMT at later times resulting from upshear-tilted organized convection. Here we seek to further understand how changes in CMT are communicated aloft to GWMT. To this end we apply the upward-propagation filter in combination with the conservation law to analyze the changes in the vertical flux of horizontal momentum in the troposphere and stratosphere. We compare the evolution in the sheared simulation (USH) to what has already been seen in the absence of shear (UNS).

a. Decomposition into upward- and nonupward-propagating signals

Recall that in the absence of background shear (i.e., the UNS simulation) the vertical flux of horizontal momentum was nearly antisymmetric about zero phase speed. In the presence of low-level negative wind shear there is a break in symmetry. Figure 10 (top) shows the vertical flux of horizontal momentum as a function of phase speed and height in the USH simulation for the two 50-h periods (left and right, respectively). The mean wind is shown in the thick black line. The shear layer leads to changes in the behavior of the convection and gravity waves such that the spectrum is no longer antisymmetric in the troposphere and stratosphere. The symmetry breaking results from enhanced vertical flux of horizontal momentum for eastward phase speeds at early times and westward phase speeds at later times. The spectrum is also broadened toward the west in part attributed to the Doppler shifting of shallow convective sources by the low-level background wind. Overall, the vertical pattern of the vertical flux of horizontal momentum is consistent with the UNS simulation. The $c > U$ portion of the spectra is qualitatively similar to that in UNS above the shear layer. In addition, for $c > U$ there is a region of negative momentum flux (the minimum at $c = 2\,\mathrm{m\,s^{-1}}$) below a region of positive flux (the maximum at $c = 5\,\mathrm{m\,s^{-1}}$). For $c < U$ there is a positive flux below a negative flux; the positive flux extends to $-10\,\mathrm{m\,s^{-1}}$ (the maximum flux occurs at $c = -3\,\mathrm{m\,s^{-1}}$), while the negative flux extends from -2 to $-18\,\mathrm{m\,s^{-1}}$ (the minimum at $c = -7\,\mathrm{m\,s^{-1}}$ at 20 km). LM10 also noted the westward skew at 5, 10, and 20 km in the mature phases of their U10 simulation (see their Figs. 8 and 9).

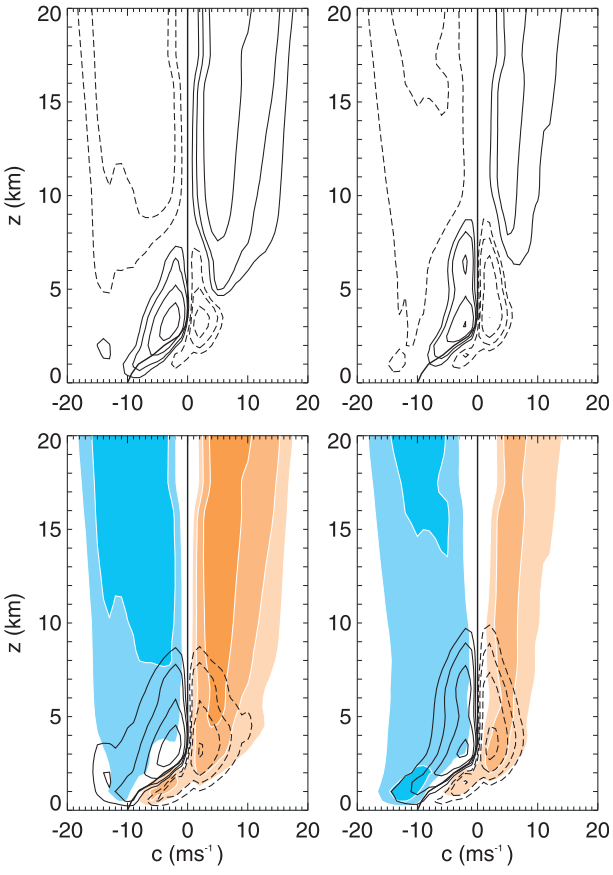

FIG. 10. Phase speed spectrum vs height during (left) 20–70 and (right) 120–170 h for (top) the vertical flux of horizontal momentum divided by density and (bottom) the spectrum separated into upward (color)- and nonupward (black)-propagating contributions for USH. Contouring as in Fig. 3.

When the vertical flux of horizontal momentum is separated into upward (color)- and nonupward (black)-propagating contributions (Fig. 10, bottom), we see a clear separation in the vertical structure. The upward flux extends from the surface up to 20 km and its sign corresponds to the sign of the intrinsic phase speed ($c - U$). The most significant change between the UNS and USH simulations is that the upward, intrinsically westward contribution is significantly broader from the surface up to 20 km during both 50-h periods. The $c < U$ nonupward flux dominates during the first period but then weakens as the $c > U$ negative flux strengthens. The strengthening of the nonupward negative flux occurs in conjunction with a strengthening of the negative upward flux in the shear layer. These changes are clearly reflected in the domain-averaged profiles that can be calculated by integrating over phase speeds. Figure 11 shows the integral of the vertical flux of horizontal momentum for $c > U$ (black) and $c < U$ (gray), including

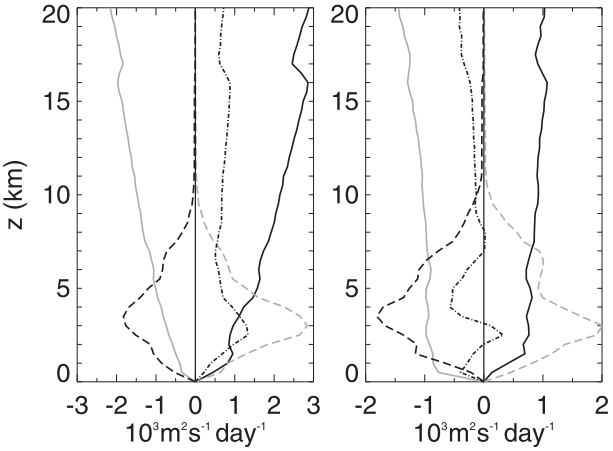

FIG. 11. Evolution during (left) 20–70 and (right) 120–170 h of the vertical flux of horizontal momentum divided by density shown in Fig. 10 integrated over $c > U$ (black) and $c < U$ (gray) phase speed for upward (solid) and nonupward (dashed) contributions for USH. The domain average flux is dashed–dotted.

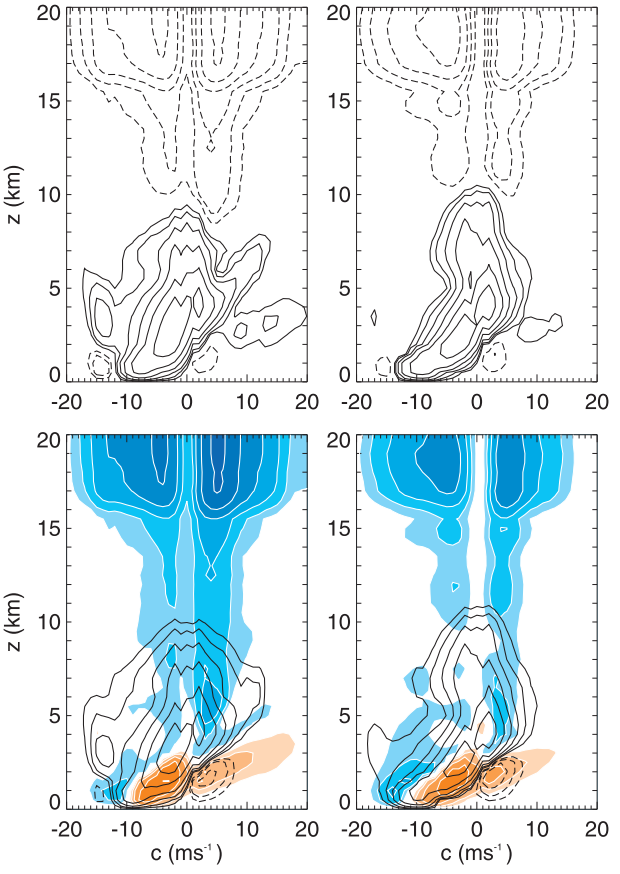

FIG. 12. Phase speed spectrum vs height during (left) 20–70 and (right) 120–170 h for (top) the vertical sensible heat flux and (bottom) the spectrum separated into upward (color)- and nonupward (black)-propagating contributions for USH. Contouring as in Fig. 5.

their upward (solid) and nonupward (dashed) contributions. The integrated profiles show the breaking of antisymmetry seen in UNS (see Fig. 4). The positive ($c < U$) nonupward contribution dominates initially but as the convection evolves the negative ($c > U$) contribution dominates. Similarly, the positive upward ($c > U$) contribution dominates initially but, as the convection evolves, the negative ($c < U$) contribution dominates. LM10 also noted the consistency between the upward and nonupward contributions and showed that the negative nonupward flux was related to upshear tilted convection that generated westward upward-propagating gravity waves (see their Figs. 11–13).

The separation of the upward and nonupward contributions suggests that the upward-propagating wave filter is able to isolate CMT and gravity wave dissipation even in the presence of low-level wind shear. The dynamical characteristics of the two components were isolated in the absence of shear using the sensible heat flux. Figure 12 shows the corresponding total vertical sensible heat flux (top) and its decomposition into upward and nonupward contributions (bottom). The nonupward contribution is dominated by a positive sensible heat flux above the shear layer, as expected for convection. Similarly, the upward contribution is dominated by negative sensible heat flux above the shear layer, consistent with dissipating gravity waves. However, within the shear layer the sensible heat flux does not have a consistent sign for either contribution. In the presence of wind shear the sign of the sensible heat transport by gravity waves cannot be considered as solely downgradient (i.e., negative). In particular, nondowngradient behavior can result from a balance in the kinetic energy equation involving the buoyancy production and shear production:

$$\theta' w' \approx \frac{\Theta}{g} \frac{dU}{dz} u' w' . \tag{6}$$

Thus, for upward-propagating waves that have the same sign intrinsic phase speed as vertical flux of horizontal momentum, production of kinetic energy by shear can lead to buoyancy production. Alternatively, convection can generate downgradient sensible heat transport through forced (stable) ascent. In particular, the forced ascent over propagating gust fronts should have negative sensible heat flux below the level of free convection. At early times (Fig. 12, bottom left) there are shallow regions of negative flux at values of $(c - U) > 0$ and $(c - U) < 0$. At later times, the negative (and nonupward) sensible heat fluxes are at positive phase speeds only, consistent with a dominance of downshear-propagating gust fronts during the more organized phases of the convection.

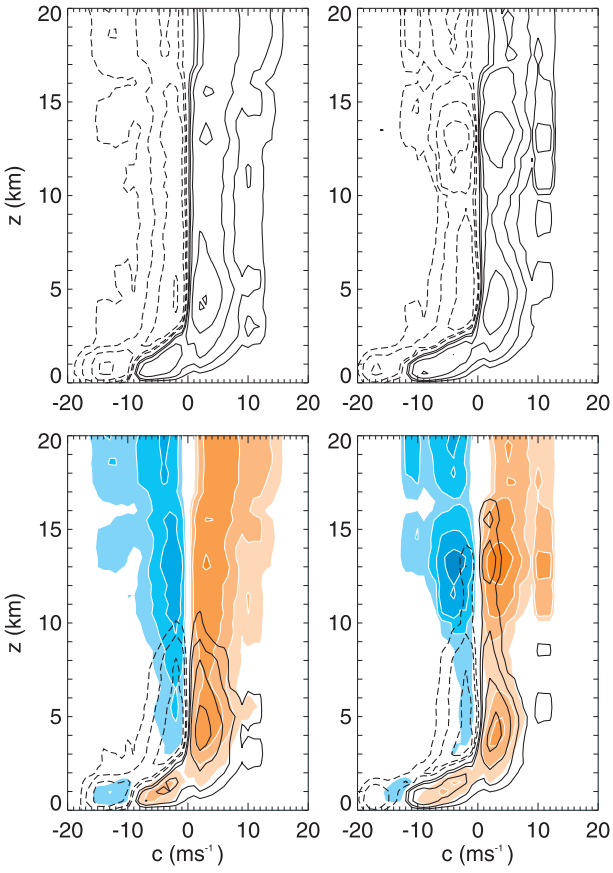

FIG. 13. As in Fig. 10, but for the pseudomomentum density divided by density A/ρ_0 for USH. Contouring as in Fig. 7.

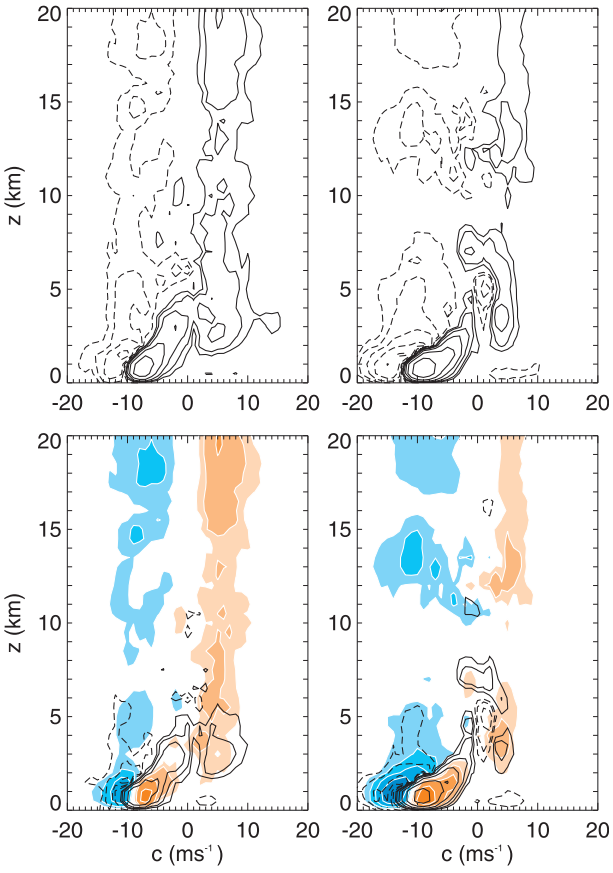

FIG. 14. As in Fig. 10, but for the transience of the pseudomomentum density divided by density $-\partial A/\partial t/\rho_0$ for USH. Contouring as in Fig. 8.

b. *Pseudomomentum budget analysis of USH*

As mentioned in the introduction, an outstanding question is how changes in CMT are connected to changes in GWMT. The changes in the vertical flux of horizontal momentum in the presence of low-level wind shear can be understood using the pseudomomentum budget. Note that in the presence of wind shear the pseudomomentum density, flux, and effective source/sink terms include a term proportional to the shear of the background flow [see (4a), (4c), and (4e)]. Above the shear layer the pseudomomentum density only involves the first two terms in (4a), similar to UNS. Figure 13 (top) shows the pseudomomentum density divided by density A/ρ_0 as a function of phase speed and height for the two 50-h periods (left and right, respectively). Recall that the pseudomomentum density is related to the vertical flux of horizontal momentum via the vertical group velocity. The psedomomentum density shows a clear Doppler shift toward higher westward phase speeds in the shear layer. The density is largest in the shear layer and ~5 km. There is a clear increase in A/ρ_0 in the region of convective outflow during the second period that is broader on the westward side. The decomposition into upward- and nonupward-propagating contributions (Fig. 13, bottom) suggests that the changes in the region of convective outflow are associated with the upward-propagating contribution and coincide with the more organized convective activity. The nonupward contribution dominates in the midtroposphere and in the shear layer.

According to the pseudomomentum budget (as described earlier), the negative time tendency of the pseudomomentum density can change the vertical divergence of the vertical flux of the horizontal momentum. Figure 14 (top) shows the negative time tendency of the pseudomomentum density $-\partial A/\partial t/\rho_0$ as a function of phase speed and height for the two 50-h periods (left and right, respectively). Overall, the tendency in the lower troposphere is very large and much larger than for UNS and it grows both in the shear layer and in the region of convective outflow. The interpretation of the transience term is that it denotes wave propagation away (decay of

wave amplitude) from a source region in the boundary layer, which leads to a divergence of momentum flux. Figure 14 (bottom) shows the decomposition into upward- and nonupward-propagating contributions. The changes in the shear layer clearly result from both upward and nonupward contributions. The broadened westward phase speed contribution corresponds to the changes in the upper stratosphere. The sign of the transience term suggests that in the shear-layer transience is a source of upward-propagating waves. These signals are consistent with generation by transient shallow convective cells in the shear layer that move at speeds close to the background wind. Transient wave generation by penetrating convective updrafts near the upper outflow region is also notable at later times, which also helps broaden the westward spectrum. This generation is consistent with a dominance of front-to-rear moving overshooting updrafts embedded within quasi-stationary upshear-tilted convective systems.

In addition to the transient changes in the pseudomomentum density, the source/sink term can also change the vertical divergence of the vertical flux of horizontal momentum. Figure 15 (top) shows the evolution of the effective source/sink term divided by the density $\tilde{S}/\rho_0$ as a function of phase speed and height for the two 50-h periods (left and right, respectively). As discussed previously, the effective source/sink term includes both nonconservative and nonlinear terms. As for UNS the nonconservative contribution is found to dominate over the nonlinear contribution (not shown). The source/sink terms exhibits a tripolar structure with height. The vertical structure becomes clearer after the upward and nonupward contributions are separated (Fig. 15, bottom). Both upward and nonupward contributions exhibit a dipole structure with height, which is skewed westward in the shear layer. The upward contribution exhibits a dipole from the surface up to 20 km and is consistent with a region of wave generation in the mid- to lower troposphere and a region of wave dissipation in the upper troposphere and lower stratosphere.[2] The nonupward contribution involves a dipole from the surface up to 12 km. The vertical structure is consistent with the transport by tilted convective structures. For $c > U$ momentum is transported from the boundary layer to the free troposphere while for $c < U$ it is in the opposite direction. Once again the overlap of the upward and nonupward source/sink terms suggests that the two contributions are coupled.

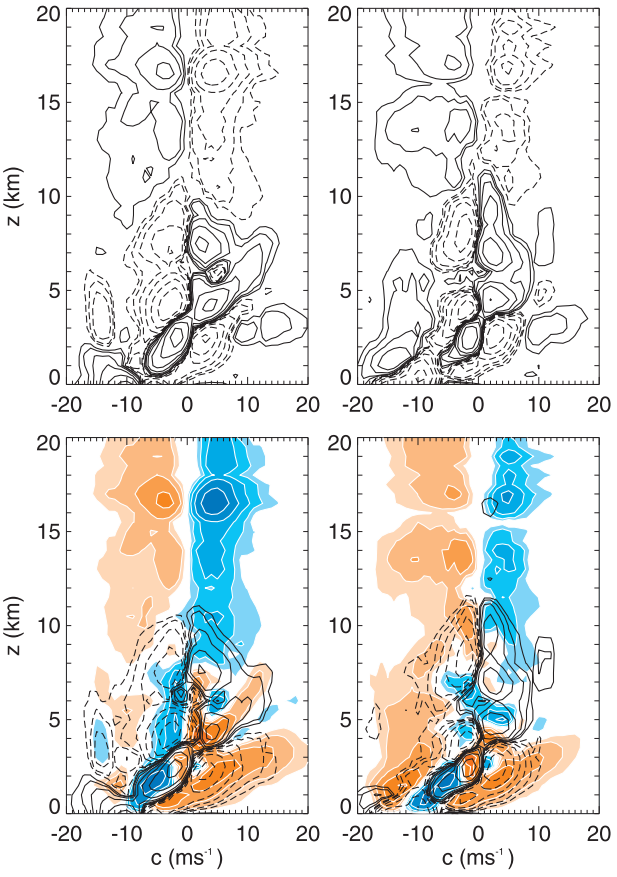

FIG. 15. As in Fig. 10, but for the pseudomomentum effective source/sink term divided by density $\tilde{S}/\rho_0$ for USH. Contouring as in Fig. 9.

Overall, the presence of low-level positive wind shear leads to a substantial change in the CMT, which is consistent with the change in convective organization. The changes in CMT coincide with enhanced GWMT from intrinsically westward waves in the convective outflow region. The changes in that region are dominated by the transience of the pseudomomentum density that is consistent with the emission of waves from the region of convective outflow. Of secondary importance is the broadening of the spectrum associated with shallow transient sources in the boundary layer. The analysis suggests that the transient sources of pseudomomentum are important for communicating the changes in the organized convective structures to the region aloft.

5. Summary and discussion

Convective momentum transport (CMT) and gravity wave momentum transport (GWMT) represent important processes in the tropical troposphere and stratosphere. Here we investigated the role of CMT and

[2] The region of wave dissipation immediately above the tropopause was found to be sensitive to vertical resolution, similar to UNS.

GWMT in two-dimensional cloud-system-resolving models. The goals were 1) to determine an objective method of separating the two contributions, which is consistent with the physical characteristics of the two components, and 2) to understand the role of transient and nonconservative diabatic and frictional processes in the vertical flux of horizontal momentum and in the connection between CMT and GWMT. To that end, we used the pseudomomentum wave-activity conservation law for two-dimensional disturbances to a vertically varying shear-stratified flow.

The first Eliassen–Palm theorem based on a linear group velocity criterion was shown to be useful for disentangling upward- from nonupward-propagating spectral elements of the vertical flux of horizontal momentum. In particular, when the linear criterion was applied it revealed that the nonupward contribution was confined to the mid- and lower troposphere, whereas the upward contribution extended from the surface to the upper stratosphere. The vertical extent of the two contributions was consistent with the expectation of convection and vertically propagating gravity waves and was applied in the absence and presence of low-level background wind shear. The physics governing the upward and nonupward contributions was also assessed using the vertical sensible heat flux. Overall, the nonupward contribution was found to be dominated by upgradient vertical sensible heat flux, consistent with unstable convection. In contrast, the nonupward contribution was dominated by downgradient sensible heat flux, consistent with damped vertically propagating gravity waves. The sensible heat flux analysis supported the conclusion that the nonupward contribution is dominated by CMT and not by downward-propagating gravity waves. The upward contribution is dominated by upward-propagating gravity waves. The results suggested that a filter based on linear theory is useful for separating CMT and GWMT and, hence, for understanding their interaction even in the nonlinear regime. This approach holds promise for future studies focused on the links between CMT and GWMT.

The question of how changes in CMT can affect GWMT was addressed by considering the roles of transient and nonconservative diabatic and frictional sources of the vertical flux of horizontal momentum. The notion that the vertical flux of horizontal momentum is connected to transience or nonconservative sources is derived from the pseudomomentum wave-activity conservation law for two-dimensional disturbances to a vertically varying shear-stratified flow. The pseudomomentum wave-activity conservation law states that changes in the vertical flux divergence of the vertical flux of horizontal momentum is associated with transient changes in the pseudomomentum density (or wave amplitude) or quasi-steady source/sink effects (i.e., diabatic heating or friction). The terms in the conservation law connect to gravity wave generation via the ''mechanical oscillator'' and ''diabatic heat source'' effects (Fritts and Alexander 2003). The conservation law was applied to the cloud-system-resolving model simulations of multiscale tropical convection to understand changes in the vertical flux of horizontal momentum and how they depended on the presence of background wind shear.

The analysis of the pseudomomentum density revealed that the dominant regions of buoyancy–vorticity correlations, which are required for the vertical flux of horizontal momentum, occur throughout the troposphere and stratosphere. Such correlations are known to be important for wave generation by penetrative convection (e.g., Lane 2008). In the mid- to lower troposphere, the buoyancy–vorticity correlations were dominated by CMT, whereas in the upper troposphere/lower stratosphere they were dominated by GWMT. As the convection evolved there were extrema in the lower troposphere and in the region of convective outflow, highlighting the importance of convective motions in these two regions.

In the absence of background wind the vertical flux of horizontal momentum was antisymmetric. It exhibited a dipole structure with height—with negative (positive) flux below positive (negative) flux for eastward (westward) phase speeds. The vertical structure of the momentum flux was consistent with the vertical structure of the nonconservative source/sink term, which suggested that it dominates the vertical structure. The upward-propagating contribution was consistent with a region of wave generation in the lower to midtroposphere and a region of wave dissipation, associated with diffusion of momentum and sensible heat, in the upper troposphere and lower stratosphere. The upward contribution was clearly responsible for transporting momentum between the lower troposphere and lower stratosphere. The nonupward contribution was consistent with the transport of momentum between the boundary layer and the midtroposphere, which occurred within organized and tilted convective structures. The significant overlap between the upward and nonupward contributions in the troposphere highlighted a region where the two contributions may interfere for a given phase speed element. While the source/sink term dominated the structure of the vertical flux of horizontal momentum, the transience of the pseudomomentum density was responsible for changes in the region of convective outflow. The role of transience in generating pseudomomentum flux was associated with transient wave generation by convection

and propagation away from the source region, which is similar to its role in generating horizontal divergence of the horizontal flux of zonal momentum in the extratropical upper troposphere (Held and Hoskins 1985). This transient behavior is akin to wave generation by penetrating convective updrafts: the so-called mechanical oscillator effect, which generates waves through the combination of linear and nonlinear processes (e.g., Fovell et al. 1992; Song et al. 2003). The dynamics of these nonlinear processes associated with overshooting convection is an ongoing area of research.

The evolution of the vertical flux of horizontal momentum in the presence of low-level background wind shear was used to understand the impact of convective organization on the momentum fluxes and the role of transience versus nonconservative processes in its generation and evolution. During the simulation with low-level wind shear the domain-averaged vertical flux of horizontal momentum changed sign from positive to negative. The evolution was found to be consistent with a similar simulation by LM10. The decomposition of the momentum flux into upward and nonupward contributions suggested that the change of sign of the vertical flux of horizontal momentum was associated with a weakening of the nonupward, intrinsically westward flux and a strengthening of the nonupward, intrinsically eastward flux. In contrast, the change of sign in the mid- to upper troposphere was associated with a weakening of the upward, intrinsically eastward flux and a broadened upward, intrinsically westward flux.

The analysis of the pseudomomentum budget for the simulation with low-level background wind shear revealed the processes underlying the change in sign with time of the vertical flux of horizontal momentum just above the tropopause. The change in sign of the net flux was associated with the changes in transience of the pseudomomentum density in the region of convective outflow. The introduction of low-level shear modifies the convective organization and updraft tilt. This analysis showed that changes in the character of those updrafts due to organization are communicated to GWMT via transient wave generation in the outflow region of storms. This result provided support for the explanation of LM10 that upshear-tilted overshooting convective updrafts are responsible for the asymmetries in the stratospheric wave spectrum, and provides insight into the mechanisms by which CMT and GWMT are linked in organized convective systems.

Overall, the results help to shed light on some of the fundamental questions related to the separation of CMT and GWMT and their interaction. The decomposition into upward and nonupward contributions using linear theory has shown that CMT and GWMT can be objectively separated. In addition, pseudomomentum diagnostics provide a useful framework for studying vertical momentum transports and their evolution. The results show that both upward- and nonupward-propagating waves can be thought of in terms of discrete spectral elements, as considered in many gravity wave drag parameterizations (e.g., Lindzen 1981; Alexander and Dunkerton 1999). Thus, it may be useful to parameterize convective momentum transport by organized convection in a similar manner. The results also reveal that the transports above and below the tropopause are inherently coupled and that transient buoyancy–vorticity correlations represent an important contribution to the pseudomomentum flux into the stratosphere. Furthermore, it is clear that vertical momentum transport on mesoscales by gravity waves and convection should not be treated independently as the two contributions overlap significantly in the vertical and are dynamically connected. In particular, CMT and GWMT should be combined when parameterizing vertical pseudomomentum transports in regions of convection in climate models and transient effects should be accounted for. While the analysis has helped to answer some of the important questions related to CMT and GWMT in a two-dimensional configuration, there are a number of remaining open questions. For example, how does the pseudomomentum budget evolve when there is vertical wind shear throughout the domain and in three dimensions? Understanding the impacts of more realistic configurations on the results presented here is the subject of future investigation.

Acknowledgments. The authors thank Dr. F. Zhang and Dr. M. Moncrieff for helpful discussions and three anonymous reviewers for their constructive comments. TAS gratefully acknowledges support from the David and Lucile Packard Foundation. TPL was supported by the Australian Research Council's Future Fellowships (FT0990892) and Centre of Excellence (CE110001028) schemes.

REFERENCES

Alexander, M. J., and T. J. Dunkerton, 1999: A spectral parameterization of mean-flow forcing due to breaking gravity waves. *J. Atmos. Sci.,* **56,** 4167–4182.

——, J. R. Holton, and D. R. Durran, 1995: The gravity wave response above deep convection in a squall line simulation. *J. Atmos. Sci.,* **52,** 2212–2226.

Carr, M. T., and C. S. Bretherton, 2001: Convective momentum transport over the tropical pacific: Budget estimates. *J. Atmos. Sci.,* **58,** 1673–1693.

Clark, G., W. D. Hall, and J. L. Coen, 1996: Source code documentation for the Clark-Hall cloud-scale model: Code version G3CH01. NCAR Tech. Note NCAR/TN-426+STR, 137 pp.

Edmon, H. J., B. J. Hoskins, and M. E. McIntyre, 1980: Eliassen-Palm cross sections for the troposphere. *J. Atmos. Sci.,* **37,** 2600–2616.

Eliassen, A., and E. Palm, 1961: On the transfer of energy by mountain waves. *Geofys. Publ.,* **22,** 94–101.

Fovell, R., D. Durran, and J. R. Holton, 1992: Numerical simulations of convectively generated stratospheric gravity waves. *J. Atmos. Sci.,* **49,** 1427–1442.

Fritts, D. C., and M. J. Alexander, 2003: Gravity wave dynamics and effects in the middle atmosphere. *Rev. Geophys.,* **41,** 1003, doi:10.1029/2001RG000106.

Haynes, P. H., 1988: Forced, dissipative generalizations of finite-amplitude wave-activity conservation relations for zonal and nonzonal basic flows. *J. Atmos. Sci.,* **45,** 2352–2362.

Held, I. M., and B. J. Hoskins, 1985: Large-scale eddies and the general circulation of the troposphere. *Advances in Geophysics,* Vol. 28, Academic Press, 3–31.

Houze, R. A., 2004: Mesoscale convective systems. *Rev. Geophys.,* **42,** RG4003, doi:10.1029/2004RG000150.

Lane, T. P., 2008: The vortical response to penetrative convection and the associated gravity-wave generation. *Atmos. Sci. Lett.,* **9,** 103–110.

——, and M. W. Moncrieff, 2008: Stratospheric gravity waves generated by multiscale tropical convections. *J. Atmos. Sci.,* **65,** 2598–2614.

——, and ——, 2010: Characterization of momentum transport associated with organized moist convection and gravity waves. *J. Atmos. Sci.,* **67,** 3208–3225.

——, and F. Zhang, 2011: Coupling between gravity waves and tropical convection at mesoscales. *J. Atmos. Sci.,* **68,** 2582–2598.

——, M. J. Reeder, and T. L. Clark, 2001: Numerical modeling of gravity wave generation by deep tropical convection. *J. Atmos. Sci.,* **58,** 1249–1274.

LeMone, M. A., 1983: Momentum transport by a line of cumulonimbus. *J. Atmos. Sci.,* **40,** 1815–1834.

——, G. M. Barnes, and E. J. Zipser, 1984: Momentum flux by lines of cumulonimbus over the tropical ocean. *J. Atmos. Sci.,* **41,** 1914–1932.

Lin, J.-L., M. Zhang, and B. Mapes, 2005: Momentum budget of the Madden–Julian oscillation: The sources and sinks of equivalent linear damping. *J. Atmos. Sci.,* **62,** 2172–2188.

Lindzen, R. S., 1981: Turbulence and stress owing to gravity wave and tidal breakdown. *J. Geophys. Res.,* **86** (C10), 9707–9714.

——, 1990: *Dynamics in Atmospheric Physics: Lecture Notes for an Introductory Graduate-Level Course.* Cambridge University Press, 310 pp.

Lipps, F. B., and R. S. Hemler, 1982: On the anelastic approximation of deep convection. *J. Atmos. Sci.,* **39,** 2192–2210.

Moncrieff, M. W., 1992: Organized convective systems: Archetypal dynamical models, mass and momentum flux theory, and parametrization. *Quart. J. Roy. Meteor. Soc.,* **118,** 819–850.

Richter, J. H., and P. J. Rasch, 2008: Effects of convective momentum transport on the atmospheric circulation in the Community Atmosphere Model, version 3. *J. Climate,* **21,** 1487–1499.

Scinocca, J. F., and T. G. Shepherd, 1992: Nonlinear wave-activity conservation laws and Hamiltonian structure for the two-dimensional anelastic equations. *J. Atmos. Sci.,* **49,** 5–27.

——, and W. R. Peltier, 1994: Finite-amplitude wave-activity diagnostics for Longs stationary solution. *J. Atmos. Sci.,* **51,** 613–622.

Song, I.-S., H.-Y. Chun, and T. P. Lane, 2003: Generation mechanisms of convectively forced internal gravity waves and their propagation to the stratosphere. *J. Atmos. Sci.,* **60,** 1960–1980.

Wu, X., X.-Z. Liang, and G. J. Zhang, 2003: Seasonal migration of ITCZ precipitation across the equator: Why can't GCMs simulate it? *Geophys. Res. Lett.,* **30,** 1824, doi:10.1029/2003GL017198.

——, L. Deng, X. Song, G. Vettoretti, W. R. Peltier, and G. J. Zhang, 2007: Impact of a modified convective scheme on the Madden–Julian Oscillation and El Niño–Southern Oscillation in a coupled climate model. *Geophys. Res. Lett.,* **34,** L16823, doi:10.1029/2007GL030637.

Zhang, G. J., and N. A. McFarlane, 1995: Role of convective-scale momentum transport in climate simulation. *J. Geophys. Res.,* **100** (D1), 1417–1426.